

Research Paper

Spider Toxin Peptide Lycosin-I Functionalized Gold Nanoparticles for *in vivo* Tumor Targeting and Therapy

Huaxin Tan^{1,2,4}, Yazhou Huang¹, Jianghong Xu², Bo Chen², Peng Zhang¹, Zhongju Ye², Songping Liang¹, Lehui Xiao^{2,3}✉, and Zhonghua Liu¹✉

1. The National & Local Joint Engineering Laboratory of Animal Peptide Drug Development, College of Life Sciences, Hunan Normal University, Changsha, Hunan 410081, China;
2. Key Laboratory of Phytochemical R&D of Hunan Province, College of Chemistry and Chemical Engineering, Hunan Normal University, Changsha, Hunan, 410081, P. R. China;
3. State Key Laboratory of Medicinal Chemical Biology College of Chemistry, Tianjin Key Laboratory of Biosensing and Molecular Recognition, Nankai University, Tianjin, 300071, China;
4. Department of Biochemistry and Molecular Biology, School of Pharmaceutical and Biological Science, University of South China, Hengyang, 421001, China.

✉ Corresponding authors: Fax: +86-022-23500201E-mail: Lehui Xiao, lehuixiao@nankai.edu.cn; Zhonghua Liu, liuzh@hunnu.edu.cn

© Ivyspring International Publisher. This is an open access article distributed under the terms of the Creative Commons Attribution (CC BY-NC) license (<https://creativecommons.org/licenses/by-nc/4.0/>). See <http://ivyspring.com/terms> for full terms and conditions.

Received: 2017.02.22; Accepted: 2017.05.08; Published: 2017.07.22

Abstract

Cell penetrating peptides (CPPs) are commonly utilized for intracellular delivery of functional materials to circumvent biomembrane barrier. However, further application of CPPs is hindered by lacking selectivity toward targeted cells. The spider venom peptide, lycosin-I, is a CPP with potent cytotoxicity to cancer cells, which might enable lycosin-I to deliver functional materials into cancer cells selectively. In this study, we demonstrated that the lycosin-I-conjugated spherical gold nanoparticles (LGNPs) not only exhibited efficient cellular internalization efficiency toward cancer cells but also displayed unprecedented selectivity over noncancerous cells. Although LGNPs were removed from the living circulatory system via reticuloendothelial system-dominant clearance modes without noticeable adverse effects to animals, they actually displayed active tumor-targeting effects and efficient accumulation in tumors *in vivo*. Furthermore, the potential application of this platform for cancer therapy was explored by lycosin-I-conjugated gold nanorods (LGNRs). LGNRs exhibited selective intracellular translocation towards cancer cells and efficient photothermal effect under near infrared (NIR, 808 nm) irradiation, which consequently killed cancer cells *in vitro* and *in vivo* effectively. Therefore, the established LGNPs and LGNRs possessed great potential in cancer-targeting delivery and photothermal therapy.

Key words: Spider anticancer peptide lycosin-I; Spherical gold nanoparticles; Gold nanorods; Intracellular delivery; Photothermal therapy.

Introduction

Though the selective permeability of phospholipid bilayer is essential to the survival and function of living cells, it is the major obstacle for effective intracellular cargo delivery especially in medical diagnosis and therapy. The penetration of polar or low soluble compounds through cell membranes needs mechanical support or chemical helper [1]. In recent years, the discovery and development of cell penetrating peptides (CPPs) have partly resolved this challenge [2]. CPPs are a class of

diverse peptides, composed of 5-30 amino acids, and can cross cell membranes *via* multiple pathways including direct translocation and energy-consuming endocytosis [3]. On the other side, the applications of CPPs as a promising intracellular transporter have been extensively studied in imaging diagnosis, gene therapy and drug delivery [4]. However, the deeper exploitations of CPPs are faced with two inevitable restrictions: nonspecificity and easy proteolysis [5]. Therefore, the discovery and design of novel CPPs

with excellent cell selectivity and stability are still in demand particularly in cancer diagnosis and therapy.

With the 2015 Nobel Prize in Physiology or Medicine being awarded to artemisinin and abamectin [6], medicinal products from natural resources have been proposed to worldwide attention again. Among them, spider venom is considered to be an ideal source of potentially active peptides due to the tremendous biochemical diversity of spider venom peptides in diverse species. Lycosin-I, a 24 amino acid peptide isolated from the venom of the spider *Lycosa singorensis*, has been proven the great potential as a novel drug candidate against malignant tumors and bacterial infection [7, 8]. Moreover, it was found that lycosin-I is able to interact with cell membranes and enter into cell plasma to activate the mitochondrial death pathway to sensitize cancer cells for apoptosis, as well as up-regulates p27 to inhibit cell proliferation [7]. In recent studies, a strong interaction between lycosin-I and lipid membrane was observed by total internal reflection fluorescence microscopy. Lipid membranes induce the formation of amphiphilic-helix conformation of lycosin-I and subsequently stable aggregates of peptide molecules on bilayer, which are believed to be crucial for the cell penetrating ability of lycosin-I [9]. More interestingly, lycosin-I showed very low effect on normal cells, such as erythrocytes, Hek293t cells, when its concentration was much higher than the dosage that could kill cancer cell lines [7]. All those findings imply the potential of lycosin-I for cancer cell-targeted intracellular transportation. To verify that, gold nanoparticles were chosen in this study as a nanoprobe to evaluate the delivery efficacy of lycosin-I to the cancer cells.

Gold nanoparticles are colloidal or clustered particles with diameters in the range of a few to several hundreds of nanometers that consist of a gold core and a functionalized surface coating [10]. The synthetic versatility of gold nanoparticles enables fine tailoring of the particle size, shape and surface properties. The size range of 1-150 nm and diverse morphologies endow different gold nanoparticles with unique chemical, electrical and optical properties. Besides, the excellent biocompatibility and versatile bioconjugation capability of gold surface make it feasible to introduce reactive functional groups that can be used in bioimaging, drug delivery, disease diagnosis and therapy. On the other side, nanoparticles are ideal platforms to protect the attached bioagents from the degradation and clearance in blood, which greatly lower the cost of large-scale synthesis especially for some short peptides [11]. Despite these advantages, gold nanoparticles are still facing grand challenges in

biomedical applications including inefficiency in cellular internalization and non-selectivity. To overcome these barriers, we conjugated lycosin-I peptides to the surface of gold nanoparticles and then explored the targeted intracellular translocation efficiency as well as potential therapeutic capability *in vitro* and *in vivo* for the first time. First, lycosin-I-modified spherical gold nanoparticles (LGNPs) were established to evaluate the enhanced intracellular delivery of nanoparticles. Cell-selective internalization of LGNPs was tested *in vitro* in 6 cell lines, and the tumor-targeted efficiency *in vivo* was also assessed in tumor xenograft mouse model. Furthermore, in order to explore the potential applications of lycosin-I-modified gold nanoparticles in cancer therapy, lycosin-I-modified gold nanorods (LGNRs) were established due to the excellent photothermal conversion efficiency of the rod shape nanostructure in the near infrared window, and the improved photothermal therapy of cancer was evaluated *in vitro* and *in vivo*.

Methods

The spherical gold nanoparticles (GNPs) used in this work were synthesized *via* a seed-mediated growth method as described detailedly in previous studies [12]. The gold nanorods (GNRs) used in this work were synthesized based on a seed-mediated growth method [13]. In brief, 220 μL of 0.01 M NaBH_4 and 37 μL of 24.28 mM HAuCl_4 were mixed with 2.7 mL of 0.1 M CTAB solution. After 2-hour incubation at 37 $^\circ\text{C}$, the gold seed solution was successfully prepared with the color of the mixture changing to deep dark brown. Then 48 μL seed solution were added into 29.31 mL of 0.1 M CTAB solution with 372 μL of 24.28 mM HAuCl_4 , 180 μL of 0.01 M AgNO_3 and 144 μL of 0.1 M ascorbic acid solution. After appropriate time of water bath at 38 $^\circ\text{C}$, the GNRs solution were concentrated by 10 times *via* centrifuge and stored at 4 $^\circ\text{C}$ before use.

Lycosin-I, TAT and S-lycosin-I were synthesized using an Fmoc (N-(9-fluorenyl) methoxycarbonyl)/tert-butyl strategy and HOBt/TBTU/NMM coupling method on an automatic peptide synthesizer (PerSeptive Biosystems) as we previously described [7, 9].

The conjugation strategy for lycosin-I and Tat peptide was referred to our previous study [12]. Briefly, 1 mL of GNPs stock solution was centrifuged at 6000 rpm for 10 min to remove the extra chemicals in the solution. The pellet was dispersed in 150 μL of 1 mg/mL BSPP solution. To graft peptides onto the nanocargo surface, 40 μL of borate buffer (50 mM, pH 8.2) and 1.2 μL of SH-PEG-NHS (20 mM) were firstly mixed together with 1.2 μL of peptides (0.13 mM)

with gently stirring for 3 h. After that, the mixture was introduced to the nanocargo solution and left to react for additional 3 h. In order to increase the stability of the nanocargo in salt solution, 5 μL of 20 mM SH-PEG-CH₃ was added to the mixture and kept stirred for another 5-8 h. Those unreacted chemicals were removed by centrifugation for three times. The peptide-modified GNPs (LGNPs) were suspended in 200 μL of deionized water and stored at 4 °C prior to use. The peptide-modified GNRs (PGNRs) were prepared in the same way. The PEG-modified GNPs (PGNPs) and GNRs (PGNRs) were prepared as the control in the study.

The size and zeta-potential of gold nanoparticles were characterized by UV-vis absorption spectroscopy and dynamic light scattering (DLS, Zetasizer Nano ZSP, Malvern, UK), respectively. The stability and dispersibility of nanoparticles were assessed by dark-field microscopy on an upright microscope (Eclipse Ni-U, Nikon, Japan). Halogen light source was focused onto the sample through an oil-immersed dark-field condenser (NA 1.43-1.20), and the scattered light from the sample were collected and captured simultaneously by a sCMOS camera (Orcaflash 4.0, Hamamatusu, Japan). The images were processed and analyzed with Image J (<http://rsb.info.nih.gov/ij/>).

HeLa (CCL-2), MAT-Ly-Lu (CRL2376), SW480 (CCL-228), Hek293t (CRL-11268G-1), HUVEC (CRL-1730) and HBL100 (HTB-124) cell lines were obtained from ATCC. Cells were seeded on 22 mm \times 22 mm clean coverslips in plastic cell culture dishes at the cell density of around $10^5/\text{mL}$. After being fully adhered, cells were incubated with gold nanoparticles in serum-free cell culture medium for 2 hours at 37 °C. The slips were carefully washed 3 times by PBS and reversely covered to glass slides for dark-field imaging.

The quantitative analysis of intracellular nanoparticle content was performed by flame atomic absorption spectrophotometer (FAAS, WFX-110, Beijing Beifen-Ruili Analytical Instrument Co., Ltd, China). In brief, the nanoparticle treated cells were collected after trypsinization. The extra gold nanoparticles in the culture medium were removed by centrifuged at the speed of 1000 rpm. After 3 time washes with fresh PBS, the cells were resuspended in 50 μL PBS. The cell number was calculated in advance by Image Cytometer (Cellometer K2, Nexcelom, USA), and were digested completely in 50 μL fresh aqua regia for 6 hours. After being pre-heated at 80 °C for 30 min, the mixtures were appropriately diluted, and the gold content in each sample were detected by FAAS (damping constant 0.4, slit width 4 nm). The standard solutions were prepared using HAuCl₄

solution at concentration of 1, 5, 10, 50, 100 $\mu\text{g}/\text{mL}$. According to the standard curve, the gold concentrations were determined. Given that the density of gold is $1.93 \times 10^7 \text{ g}/\text{m}^3$, and the volume of single gold nanosphere with diameter of 60 nm is $1.13 \times 10^{-22} \text{ m}^3$ ($V_{\text{sphere}} = 4\pi r^3/3$), the mass of single gold nanosphere is $2.19 \times 10^{-15} \text{ g}$ ($M = \rho V$). The average number of gold nanosphere in a single cell was calculated by dividing the determined gold amount by cell number. Each sample was tested 3 times for statistical analysis.

The cells were seeded at $1 \times 10^5 / \text{mL}$ in DMEM containing 10% (v/v) FBS. Aliquots, 90 μL of this suspension, were seeded into a 96-well microplate, which contained 10 μL of gold nanoparticle solution at various concentrations. The efficacy of tested nanoparticles on cell viability was determined by MTT assay as described before [7] after the cells were incubated at 37 °C for 24 hours.

All of the animal experiments in this study were performed in compliance with the guide for care and use of laboratory animals.

Healthy female 4 to 6 week-old BALB/c mice (Slac & Jingda Corporation of laboratory animals, Changsha, China) were housed under standard approved conditions and provided daily with sterile food and water *ad libitum* for 5-7 days before experiments. The study was conducted with two groups of five mice each. Mice received an intraperitoneal injection (IP) or intravenous injection (IV) of 200 μL of sterilized saline containing 200 μg LGNPs. Control group of mice was injected with isopyknic sterile saline. After 24 hours, the animals were sacrificed through CO₂ asphyxiation. Blood and vital organs including heart, liver, spleen, lung, kidney, brain, pancreas and bladder were collected appropriately. Organs were carefully washed by saline to remove the residual blood on their surfaces and dried out by filter papers. For quantification of gold in mice, tissue sections were weighed and digested in fresh aqua regia overnight. The uptake of gold was measured by FAAS as mentioned above.

In order to assess the tumor-targeting efficacy of LGNPs *in vivo*, HeLa tumor xenograft models were established. 4-6 week-old male BALB/c nu/nu mice were purchased from Model Animal Research Center of Nanjing University. 200 μL of $10^8/\text{mL}$ HeLa cells suspended in sterile saline were subcutaneously injected into the right back of each mouse. When tumors reached the size of 5 \times 5 mm in each dimension, mice were divided into 4 groups of five animals each. Each group of mice was injected 200 μL of LGNPs or PGNPs (10 mg/kg) *via* IT injection or IP injection, respectively. Control group of mice was injected with isopyknic sterile saline. After 24 hours,

the animals were sacrificed through CO₂ asphyxiation. The tumor tissues and main organs were harvested and treated as described above. The gold contents in tumors and normal tissues were measured by FAAS as mentioned above.

HeLa cells were seeded in a 96-well plate at a density of 10⁴ cells per well and incubated overnight at 37 °C. 100 µL of LGNRs or PGNRs at the final concentration of 16 µg/mL were added into the wells, respectively, while control group were added fresh cell culture medium. After 2-hour incubation, the cell culture solution containing LGNRs or PGNRs was replaced by fresh complete DMEM medium. Subsequently, cells were divided into 2 groups and were treated with near-infrared irradiation (808 nm) at a power density of 2 W/cm² or 5 W/cm², respectively for 5 minutes by Fiber Coupled Laser System (STLXXYY-ZZW, STONE Laser, Beijing, China). After irradiation, the cells were cultured for another 24 hours, and then the cell viability was examined by MTT assay. To verify the cancer cell specificity of LGNRs photothermal efficacy, Hek293t cells were chosen as noncancerous cell control.

HeLa tumor xenograft models were established as described above to evaluate the photothermal efficacy of LGNRs in tumor ablation. BALB/c nude mice with HeLa tumor xenograft were randomly separated into 3 groups with 5 mice each, and were intravenously injected with 10 mg/kg LGNRs, PGNRs and sterile PBS three times with a time interval of 3 days, respectively, when the size of tumor in each animal reached 5×5×5 mm in each dimension. The tumor sites of each mouse were irradiated by 808 nm laser at power density of 3.54 W/cm² for 5 minutes at a time point of 24 hr and 48 hr after each injection [14]. The length and width of tumors and the body weight of mice were measured every 3 days. The respective tumor volumes were calculated with the following formula: volume=width² (cm²) × length (cm)/2. After 19 days, tumors were excised, weighted and prepared for transmission electron microscope detection (JEM-1200 EX, JEOL, Japan).

Results

Cell-specific Internalization of LGNRs

The fabrication and modification of spherical GNPs were achieved *via* gold-thiol chemistry as described in the early study [12]. The stable conjugation of lycosin-I was further confirmed by UV-vis absorption spectroscopy and dynamic light scattering as shown in **Figure S1**. Negligible size change of GNPs was found after the peptide conjugation. Moreover, the morphology and

monodispersity of LGNRs in various physiological solutions were verified by TEM (**Figure S2**) and dark-field microscopy (**Figure S3**), respectively.

The cellular uptake of LGNRs was characterized in 6 different cell lines including 3 malignant cell lines (HeLa, Mat-LyLu and SW480 cells) and 3 nonmalignant cell lines (HBL-100, Huvec and Hek293t cells). Tat peptide (transacting activator of transcription peptide from human immunodeficiency virus 1), as one of the most commonly studied CPPs, was selected as a positive control peptide owing to the unprecedented cellular uptake efficiency after conjugated to nanoparticles (TGNPs) with different size or shape in various cell lines [12, 15-17]. Considering the instability of bare GNPs, PEG (SH-PEG-CH₃)-modified GNPs (PGNRs) were prepared as the negative control to determine the non-specific cellular uptake background. As shown in **Figure 1A left**, LGNRs and TGNPs both exhibited high cell penetrating activities in three tested cancer cell lines according to the strong scattering light from the cells, while PGNPs were hardly found in cells, which was consistent with previous studies [18-21]. By changing the focal planes, LGNRs or TGNPs were found in different spaces within the treated cells. Through quantitative analysis of the gold content inside the cell by flame atomic absorption spectroscopy (see the experimental section), the number of intracellular LGNRs, TGNPs or PGNPs were determined as showed in **Figure 1B**. After lycosin-I functionalization, uptake efficiency of GNPs increased at least 26 times. It is worth to note that LGNRs and TGNPs showed comparable intracellular internalization with no significant differences towards these tested cancer cell lines. The intracellular distribution of LGNRs in HeLa cells were displayed in **Figure S4**, which ensured the intracellular translocation of LGNRs at different time points.

Our previous work indicated that, compared with cancer cells, noncancerous cells were much less sensitive to lycosin-I possibly because of reduced interaction between lycosin-I and their membrane [7]. We wondered if this characteristic of lycosin-I could be transmitted to LGNRs. Here we tested the cellular uptake efficiency of LGNRs with another 3 non-tumor cells. As shown in **Figure 1A right**, the uptake efficiencies of LGNRs were dramatically decreased in these non-tumor cells. No statistical difference was found between LGNRs- and PGNPs-treated cells. On the contrary, TGNPs still maintained high efficiency in intracellular translocation to these noncancerous cells (**Figure 1B, lower**). These results from TGNPs were consistent with previous studies of Tat-modified nanoparticles [15, 22]. According to these results, though traditional CPPs possess excellent cell

penetrating activity, the further applications in cancer diagnosis and therapy are impeded by lacking effective selectivity toward targeted cancer cells. While in the case of LGNPs, the LGNPs intake by HeLa cells was 91 times higher than that by Hek293t cells. Moreover, the uptake of LGNPs was further investigated in two primary mammalian cells, rat cardiocytes and hippocampus neurons. As shown in **Figure S5**, LGNPs but not TGNPs kept impermeable in these two cells. Taking together, these data indicate that the surface-modification by lycosin-I endowed nanoparticles with not only high cell penetrating activity but also excellent selectivity towards cancer cells over noncancerous and normal cells.

The Mechanism of Cellular Uptake of LGNPs

In order to explore how lycosin-I determined the efficacy and selectivity of LGNPs intake by cancer cells, the sequence scrambled peptide (S-lycosin-I), with inverted amino acid sequence of natural lycosin-I, was synthesized and covalently conjugated on the surfaces of GNPs following the same modification strategy (SLGNPs). As expected, S-lycosin-I was not toxic to HeLa cells even at the concentration of 50 μM , while lycosin-I killed nearly half of cells at the concentration of 10 μM (**Figure 2A**). No obvious cytotoxicity was detected until the final

concentration of lycosin-I increasing to 25 μM , which was consistent with our previous results of lycosin-I with selective antitumor activity. However, S-lycosin-I lost cytotoxicity in both cells. As shown in **Figure 2B**, unlike LGNPs, SLGNPs did not discriminate between cancer and noncancerous cells with similar amounts of SLGNPs detected in individual HeLa and Hek293t cell according to the statistical analysis. Additionally, although intracellular SLGNPs were significantly decreased compared to LGNPs in HeLa cells, they still possessed significantly higher penetrating activity than PGNPs in HeLa cells. Lycosin-I and S-lycosin-I shared identical amino acid composition and therefore the same cationic charges and hydrophobicity which are important to the penetrating activity of CPPs, but they had distinct amino acid sequences and conformations. As shown in **Figure S6**, S-lycosin-I showed a random coil structure with or without lipids, while lycosin-I displayed obvious α -helical structure in the presence of POPC [9]. Our data demonstrate that the amino acid sequence and specific conformation of lycosin-I are not only essential for its bioactivity, but also decide the intracellular uptake efficiency as well as the cell selectivity of LGNPs.

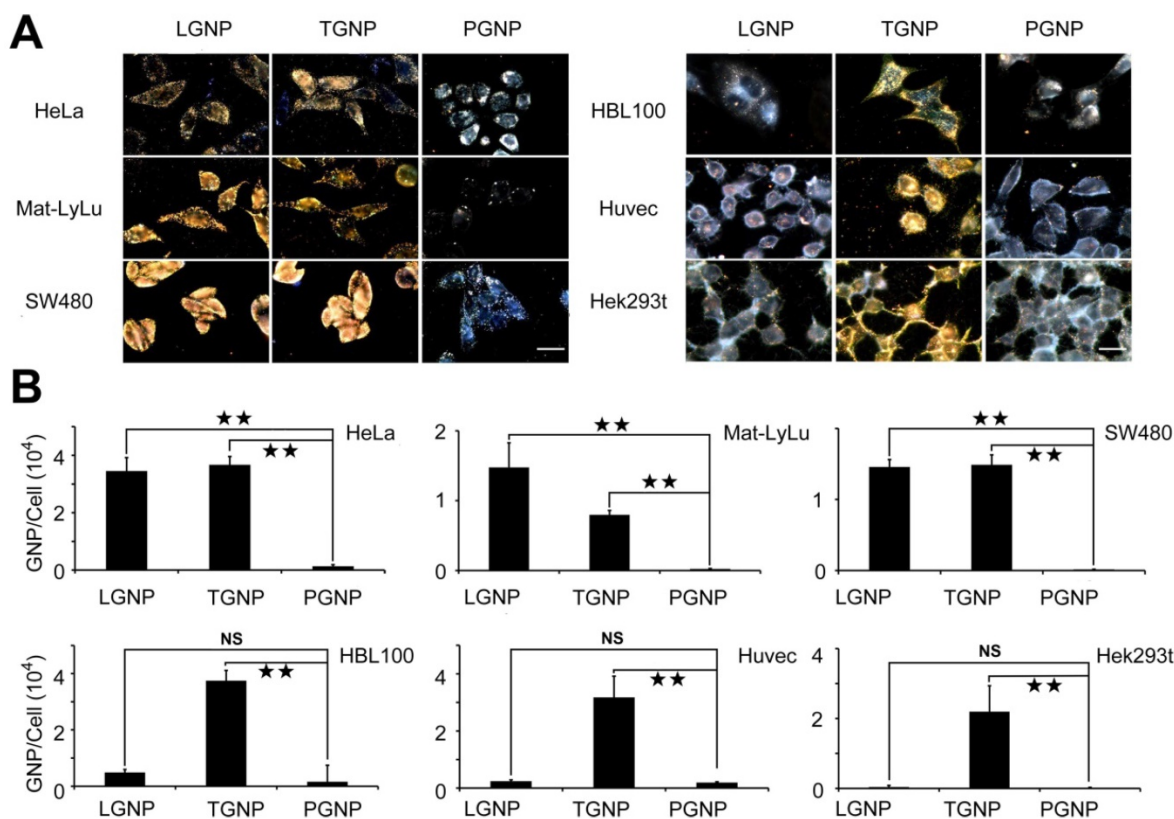


Figure 1. The evaluation of cell penetration of LGNPs. A) Dark-field light scattering images of cells treated with LGNPs, TGNPs and PGNPs. B) Quantitative analysis of cellular intake of LGNPs, TGNPs and PGNPs determined by AAS (mean \pm SD, n=3). Statistical significance is indicated by \star (p-value <0.05), $\star\star$ (p-value <0.01) and NS (no significant difference). The scale bar represents 20 μm .

As revealed by the kinetic intracellular translocation results (Figure S7), the uptake of LGNPs by cancer cells was positively correlated with nanoparticle concentration or incubation time. To determine the pathways involved in LGNPs internalization, low-temperature treatment was designed to inhibit the energy-dependent endocytic process due to the deactivation of ATPase. As shown in Figure 3A and 3B, a significant decrease (~80%) in LGNPs intracellular uptake at 4 °C was found in contrast to that at 37 °C (Figure 3E), indicating receptor mediated endocytosis (RME) was the dominant pathway for LGNPs internalization [23].

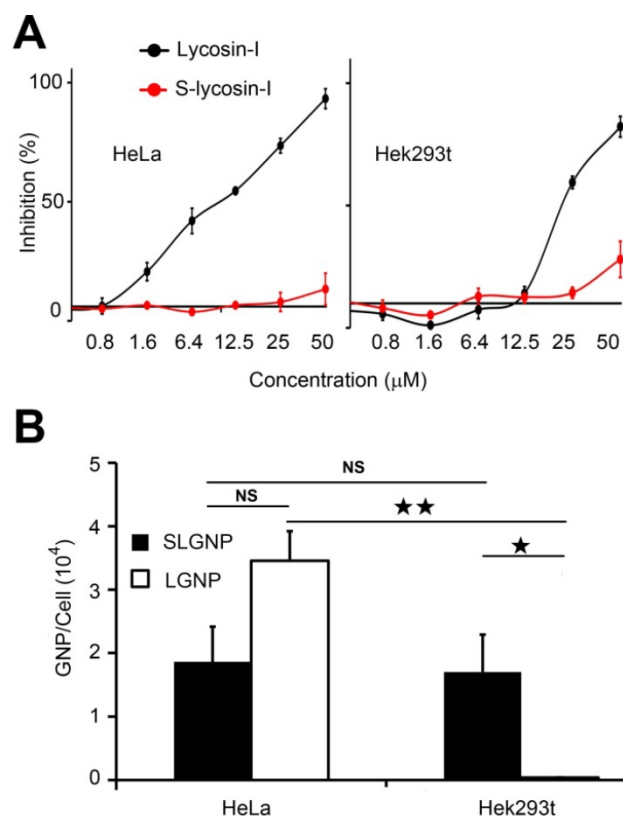


Figure 2. A comparison experiment of intracellular uptake between LGNPs and SLGNPs. A) Cytotoxicity of lycosin-I and S-lycosin-I against HeLa cells (left) and Hek293t cells (right). B) Quantitative analysis of cellular intake of LGNPs and SLGNPs determined by AAS (mean±SD, n=3). Statistical significance has been indicated by ★ (p-value <0.05), ★★ (p-value <0.01) and NS (no significant difference).

Further understanding of LGNPs uptake mechanism was achieved by pretreating HeLa cells with two well-known biochemical inhibitors of RME, dynasore (an inhibitor of clathrin-mediated endocytosis by deactivating dynamin-GTPase) [24] and genistein (an inhibitor of caveolae-mediated endocytosis by deactivating isoflavone tyrosine kinase) [25]. As shown in Figure 3E, 51.1% of LGNPs uptake was impeded by dynasore, while 58.3% of LGNPs uptake decline were observed in genistein

treated cells, compared with the data from cells treated with 32 μg/mL LGNPs in the absence of inhibitors. However, no complete inhibition was found in these two inhibitor treatments as that in the case of low temperature experiment. Altogether, these results suggest that the cellular internalization of LGNPs by HeLa cell was regulated in a complex way where both clathrin- and caveolae-mediated endocytosis processes might be involved. The cell cytotoxicity effect of LGNPs to HeLa cells was also explored. As illustrated in Figure S8, negligible cytotoxicity was observed even under the mass concentration of 128 μg/mL, which is comparable to that of PGNPs.

The Tumor Targeting Effect of LGNPs *in vivo*

Then the bio-distribution of LGNPs was first studied in normal mice. As shown in Figure 4A, LGNPs were mainly found to accumulate in spleens and livers *via* intravenous (IV) or intraperitoneal (IP) injection of 200 μg LGNPs/mouse. In IV groups, the amounts of LGNPs in spleens and livers were 35.73±17.86 μg/g and 6.20±3.17 μg/g, respectively, while in IP groups, the corresponding data were 41.89±16.44 μg/g and 7.19±0.11 μg/g, respectively. Besides, few nanoparticles were found in the brain, heart, lung or other organs after IV injection. In contrast, more amounts of LGNPs were detected in those organs after IP injection of LGNPs, which might arise from intraperitoneal circulation and altered lymphatic clearance [26]. Notably, total contents of LGNPs detected in all tissues *via* IV and IP injection were 14.6±6.04 μg and 28.0±5.43 μg, respectively, which were much lower than the initial injection amounts of 200 μg. The relative bio-distribution of LGNPs in normal mice from different organs was showed in Figure S9, and the absolute contents of LGNPs in normal mice were displayed in Table S1.

Next, the bio-distribution of LGNPs was further examined in tumor-bearing mice. Tumor xenograft of HeLa cells were established in nude mice and the amounts of nanoparticles in tumors and other main organs were determined 24 hr after IV injection of LGNPs or PGNPs at the dose of 10 mg/kg body weight (Figure 4B). LGNPs were detected mostly in tumors and spleens with amounts of 254.19±56.33 μg/g and 211.20±49.29 μg/g, respectively. In PGNPs control groups, the highest accumulation of nanoparticles was found in spleen, followed by tumor and liver. This may be attributed to the higher filtering efficacy of spleen and the presence of higher number of phagocytic cells and capillary beds in liver [27]. The absolute contents of LGNPs and PGNPs within tumor-bearing mice were displayed in Table S2. In spite of the clean effect of reticulo endothelial

system (RES, including spleen and liver), the active translocation of LGNPs into cancer cells is crucial for their specific tumor-targeting and accumulation. The uptake efficiency of LGNPs in tumor tissue was approximately 8 times higher than that of PGNPs with statistical significant difference ($p=0.0061$, $n=5$). In addition, if LGNPs or PGNPs was injected into tumors directly (IT injection), most nanoparticles were deposited in tumors, with significantly higher accumulations than those in IV injection due to the direct contact of nanoparticles and tumors. Note that more LGNPs were still detected than PGNPs in tumors although no statistic difference was observed. Together, these results verified the safety and efficient tumor-targeted translocation of LGNPs *in vivo*.

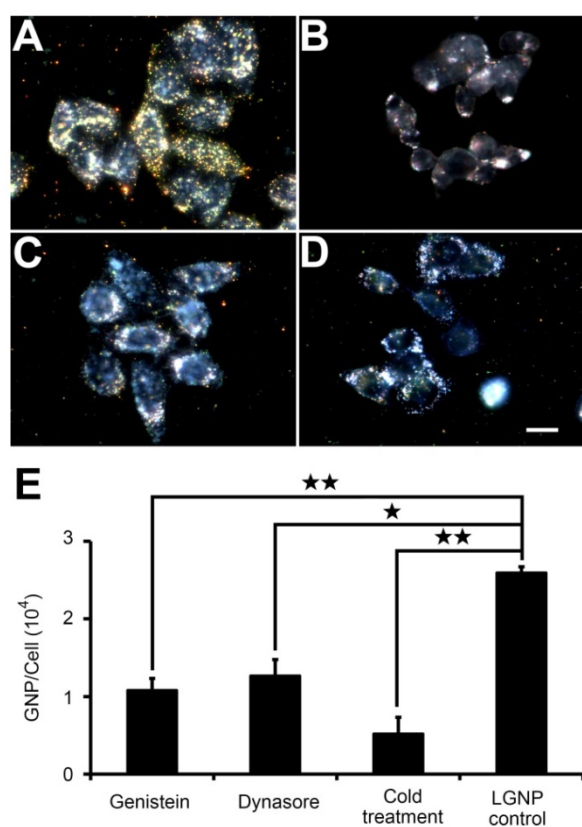


Figure 3. The intracellular uptake of LGNPs through endocytosis. Dark-field light scattering images of cells treated with LGNPs at 37 °C (A), 4 °C (B), as well as with pretreatment of dynasore (C) and genistein (D) at 37 °C. E) Quantitative analysis of cellular uptake of LGNPs by AAS (mean \pm SD, $n=3$). Statistical significance has been indicated by * (p -value <0.05), ** (p -value <0.01) and NS (no significant difference). The scale bar represents 10 μ m.

Photothermal Therapy Effect of LGNRs on Cancer Cells *in vitro*

The tumor-targeting effect of LGNPs endowed lycosin-I-modified gold nanoparticles promising applications in drug delivery, cancer diagnosis and therapy. In this study, the potential application in cancer therapy was explored by establishing a LGNRs

system because the rod shape nanostructure has excellent photothermal conversion efficiency in the near infrared window, which guarantees deep tissue penetration depth for *in vivo* applications. After 2-minute exposure to NIR irradiation (808 nm, 5 W/cm²), the temperature of LGNRs solution rose to around 53 °C just like bare GNRs, while blank solution without GNRs still kept at room temperature of 20 °C under the same illumination condition (Figure S10), which indicates LGNRs retained the photothermal effect. It is worth to note that LGNRs also displayed high and selective intracellular uptake toward cancer cells. As shown in Figure 5A, a statistically averaged dosage of 187 pg gold was detected in a single HeLa cell when cells were incubated with 32 μ g/mL of LGNRs for 2 hrs, which is much higher than that in PGNRs-treated HeLa cells (5.23 pg gold per cell). However, in Hek 293t cells, the uptake efficiency of LGNRs was significantly reduced to 21.4 pg gold per cell under the same condition. These results imply that the shape variation of peptide-conjugated nanoparticles did not affect the intracellular uptake efficiency and selectivity *in vitro*.

Given that the intracellular LGNRs still maintain the potent photothermal efficiency, the viabilities of those cells containing enough LGNRs should be irreversibly impaired due to the heat generated by NIR irradiation. To prove that, the cell viabilities were measured after different treatments and the data were shown in Figure 5B. Note that the cell viabilities in PBS control without irradiation were set as 100%. No significant effect was found on HeLa and Hek293t cells after exposure to NIR irradiation, indicating that the continuous-wave laser did not affect cell viability in our experimental condition. In the case of LGNRs-treated HeLa cells, the cell viabilities were significantly declined. After low-intensity of laser (2 W/cm²) treatment, 75.4% of HeLa cells were killed, while only 8.9 % of HeLa cells survived with the slightly increased intensity of laser irradiation (5 W/cm²). In contrast, in LGNRs-treated Hek293t cells, cells were much less sensitive to the laser irradiation. No statistical difference in cell viabilities was found in the presence and absence of irradiation even at the intensity of 5 W/cm². In a comparison with these two cells treated with LGNRs under the same irradiation conditions, the cell viability of Hek293t cells (88.9%) was obviously higher than that of HeLa cells (24.6%) at laser intensity of 2 W/cm² ($p=0.0067$, $n=3$). The difference was even more significant at the intensity of 5 W/cm² ($p=0.00021$, $n=3$). Notably, no significant difference was detected between PGNRs-treated HeLa and Hek293t cells under various intensities of irradiation, which might be ascribed to inadequate heat produced by relatively few amounts of

intracellular PGNRs. These results further confirm the selective intracellular translocation of LGNRs in these two kinds of cells, and also revealed the potential of LGNRs in cancer cell-selective killing through photothermal conversion.

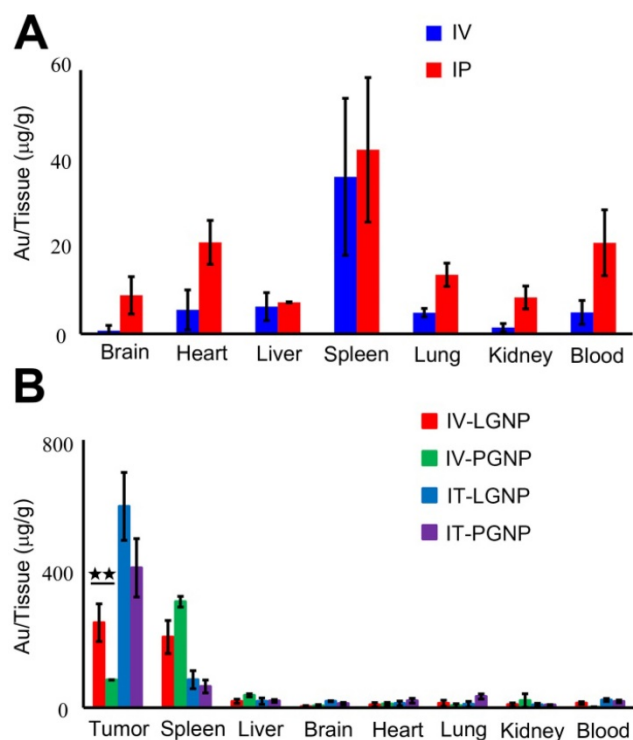


Figure 4. The tumor-targeting effect of LGNPs *in vivo*. A) Bio-distribution of LGNPs in normal mice. B) Bio-distribution of LGNPs in tumor-bearing mice. Nanoparticles were injected into mice *via* administration routes of intravenous (IV), intratumor (IT) or intraperitoneal (IP) injection (mean \pm SD, n=5). Statistical significance has been indicated by $\star\star$ (p-value <0.01).

It is worth noting that the final concentration of remaining lycosin-I on LGNRs was 1.24 μ M at most, assumed all peptides were conjugated on the surfaces of GNRs during the modification process, which is much lower than the IC₅₀ value (10 μ M) of lycosin-I against HeLa cells [7]. In this view, the LGNRs nanosystem remarkably enhanced the anticancer potency of bare lycosin-I peptides.

Photothermal Ablation Effect of LGNRs on Tumor *in vivo*

The photothermal effect of LGNRs on tumor ablation *in vivo* was further studied in HeLa tumor xenograft model. Mice bearing tumors were treated with IV injection of 10 mg/kg LGNRs, PGNRs or sterile PBS for three times every 3 days, followed by NIR irradiation at the tumor site by 808 nm laser at intensity of 3.54 W/cm² for 5 minutes at 24 hr and 48 hr post-injection. As shown in **Figure 6A**, the growth of tumor was completely stagnated by the IV injection of LGNRs, while that of PGNRs-injected mice was just

partly delayed compared with negative controls (with injection of PBS) during the therapeutic period. This conclusion was also supported by the excised tumors and their average weights as displayed in **Figure 6B** and **6C**. As revealed by the statistical analysis of tumor weights, significant differences were observed when LGNRs group was compared with PGNRs group (p<0.001) and PBS group (p=0.028), respectively. The p-value between PGNRs and PBS groups was calculated as 0.081 (no statistical difference). The data indicates that it was the LGNRs treatment that actually caused the inhibition of tumor growth *in vivo*.

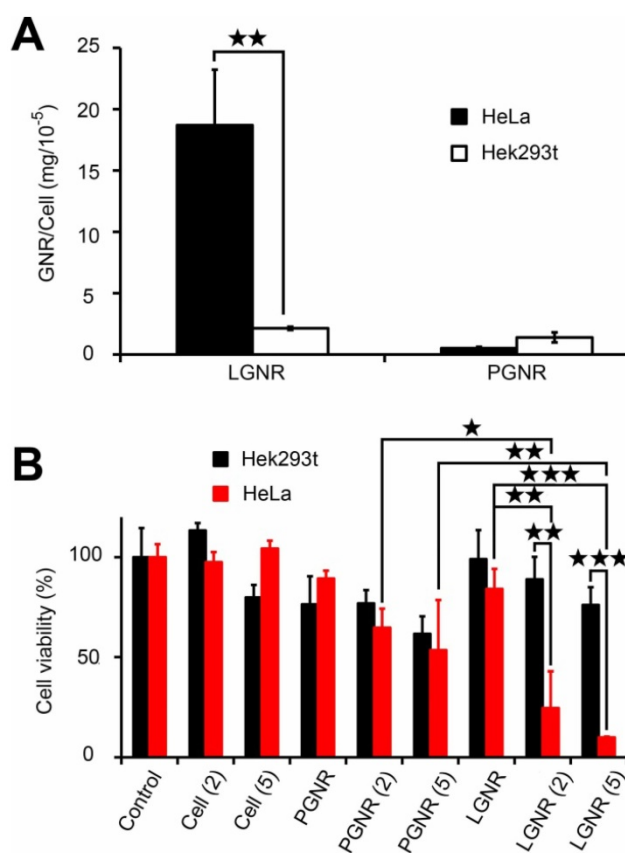


Figure 5. Selective cellular internalization of LGNRs by cancer cells and cell viability assay *via* photothermal effect. (A) The intracellular translocation of LGNRs in HeLa and Hek293t cells. (B) The photothermal killing effect of LGNRs on HeLa and Hek293t cells after NIR irradiation at various power densities of 0 (no laser), 2 or 5 W/cm² (mean \pm SD, n=5). Statistical significance has been indicated by \star (p-value <0.05), $\star\star$ (p-value <0.01) and $\star\star\star$ (p-value <0.001).

The tumor tissues of each group were fixed and sliced for transmission electron microscopy (TEM) examination. **Figure S11** clearly showed that the intracellular LGNRs scattered in the cytoplasm, while PGNRs were mostly clustered in vesicles with evidently reduced amounts. Consequently, in spite of the “ablation” of tumors caused by the passive accumulation of nanorods, LGNRs still possessed the

superiority in photothermal therapy *in vivo* for their active tumor-targeting effect. Additionally, the mice in all three groups maintained a stable body weights during the therapeutic period (Figure 6D), which suggests that both LGNRs and PGNRs had negligible toxicity. All of these results substantiated the potential of LGNRs in cancer photothermal therapy.

Discussion

Efficient intracellular delivery of nanoconjugates is the primary issue to be considered in medical nanotechnology. Though, CPPs have been used in improving cell-penetrating activities of conjugated nanocargoes, their further application was still hindered by low cell selectivity especially in cancer therapy. The established LGNRs show enhanced efficiency in intracellular uptake and accumulation in three cancer cell lines, but remain inefficient in translocation into tested noncancerous cells compared to the typical CPP Tat peptides-coated nanoparticles. The positive charge of both lycosin-I and Tat peptides is believed to be the main reason for their high cellular translocation efficiency. Numerous studies have shown that surface charge has a significant impact on cellular internalization of a variety of nanocarriers [25], which was also confirmed by the data from SLGNPs. Cationic nanoparticles

generally enter into cells with higher efficiency than the anionic counterparts owing to their higher affinity toward cell membranes [28, 29]. In this study, the cationic peptides conjugated on the surfaces of GNPs facilitated the interaction with cell membranes and resulted in highly efficient intracellular translocation. On the other hand, the cancer cell-selective uptake of LGNRs in cancer cells makes lycosin-I more attractive in targeted delivery than many other CPPs identified so far. In most studies, elaborate designs are essential to accurately activate the cell penetrating ability of CPP-coated cargos after they approach targeted cells or tissues [30, 31]. Otherwise, the non-specific intracellular translocation of nanocargoes will not only reduce their efficiencies to targeted cells, but also cause serious side effects sometimes. In the comparison experiment between LGNRs and SLGNPs, LGNRs demonstrate much higher penetrating activity and selectivity on cancer cells than SLGNPs, which suggests that the unique amino acid sequence and conformation of lycosin-I might essentially account for its distinct selectivity and cell penetrating activity. In fact, similar studies also have found some peptides with certain α -helical structures could facilitate associated nanoparticles to selectively enter tumor cells [22, 32].

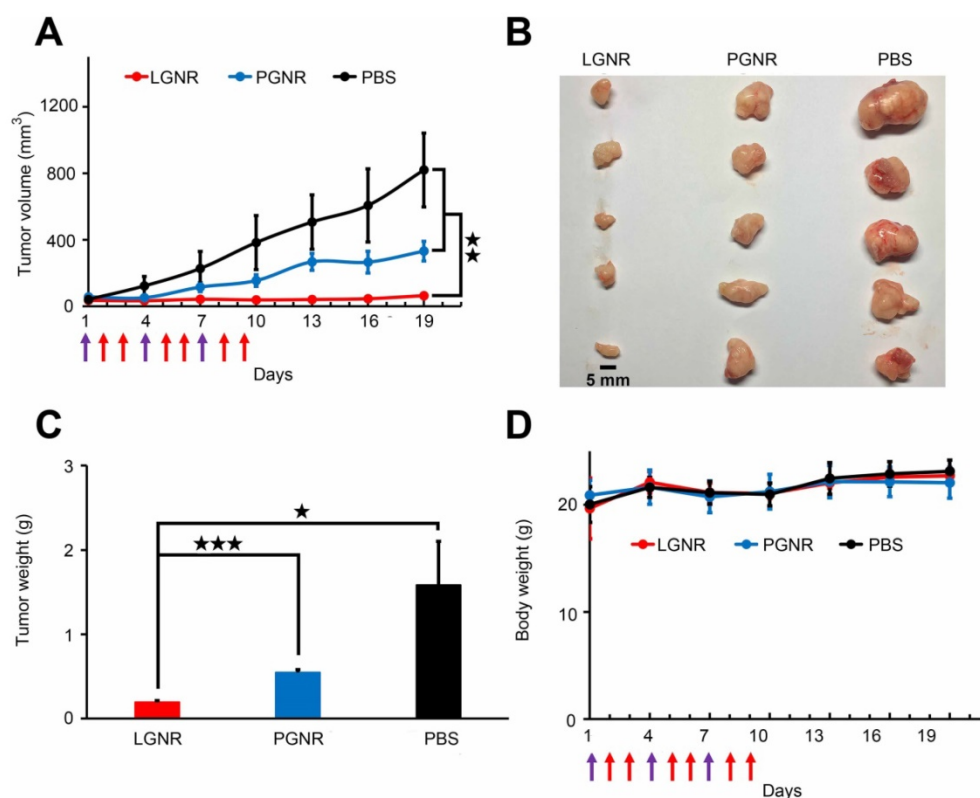


Figure 6. *In vivo* photothermal therapy of tumors by using LGNRs. A) Photographs of excised tumors from mice sacrificed at the 18th day. B) The evolution of tumor volume for animals with different treatments during the therapeutic period. Purple arrows present the injection time points and red ones indicate the NIR irradiation time points. C) The average weights of excised tumors. D) The body weight changes of animals during the therapeutic period. The data were expressed with mean \pm SD (N=5). Statistical significance has been indicated by \star (p-value <0.05), $\star\star$ (p-value <0.01), $\star\star\star$ (p-value <0.001) and NS (no significant difference).

As we found in early works, the aggregates of lycosin-I forming on the membranes were immobile and involved the interaction between lipid and peptide, which is in accordance with the 'toroidal' pore model. This membrane action mode was believed to account for cancer cell selectivity of lycosin-I. Firstly, the alteration of phospholipid composition on cancerous cell membranes will intensify the membrane interaction of lycosin-I. The negatively charged phospholipid, such as phosphatidylserine (PS) and phosphatidylethanolamine (PE), translocate and redistribute on the outer leaflet of cell membranes during cell cancerization. Those phospholipids not only provide binding sites for cationic peptide, but also participate in the formation of 'toroidal' pores [33]. Secondly, abundant microvilli on cancer cells broaden the surface area of cell membranes and provide more binding sites for lycosin-I [34]. Thirdly, the increased mobility of cancerous cell membranes will facilitate the aggregation and pore-forming of lycosin-I. Additionally, the exceeding contents of negatively charged glycosyls (such as sialic acid residues and heparan sulfates) in cancerous cell membranes also promote the electrostatic attraction between cancer cells and cationic peptides [35]. However the specific cell-selective mechanisms of lycosin-I functionalized gold nanoparticles, which are probably endowed from the lycosin-I itself, still need further investigation.

In the *in vivo* study, LGNPs were proved to effectively accumulate in tumor tissues, as excessive LGNPs were eventually eliminated *via* RES dominant clearance modes [23, 26]. Meanwhile, GNPs themselves possess great application prospects for cancer diagnosis and therapy owing to their unique optical properties and biocompatibility. Wang *et al.* designed cationic surface modified GNPs with enhanced cellular uptake as a novel radio-sensitizer to lower the effective dose of X-ray in cancer radiation therapy [36]. Chien *et al.* used GNPs as contrast agents for X-ray imaging of tumor growth *in vivo* based on the extinction effect of GNPs [37]. In this study, LGNRs were designed for further application in cancer photothermal therapy. The surface plasmon field enhancement of the absorption of GNRs is predicted to be the strongest of all the different shapes of gold nanoparticles [38, 39]. By adjusting the aspect ratios of GNRs, it is feasible to tune the absorption wavelength to the NIR region, which maximizes the conversion efficiency from light to heat [40]. In photothermal ablation of solid tumors, the NIR light provides deep-tissue penetration with high spatial precision without damaging normal biological tissues due to the low-energy absorption of NIR light by

normal tissues [41]. As expected, LGNRs efficiently and selectively enter cancer cells, and kill cancer cells by photothermal conversion effect under NIR irradiation *in vitro* and *in vivo*. As a consequence, the established LGNPs and LGNRs in this study provide a stable, efficient and tumor-targeting delivery platform *in vitro* and *in vivo*, which would be significant for practical applications in cancer diagnosis and therapies.

Acknowledgment

This work was supported by NSFC (31370783, 31670783, 31370854, 31570782, 21405045 and 21522502), Program for New Century Excellent Talents in University (China, NCET-13-0789) and Hunan Natural Science Funds for Distinguished Young Scholar (14JJ1017 and 14JJ1018), the Cooperative Innovation Center of Engineering and New Products for Developmental Biology of Hunan Province (No. 20134486).

Author Contributions

H. T., Y. H. and J. X. contributed equally to this work. H. T., Y. H., J. X., B. C., P. Z., Z. Y., and L. X. did the experiments and H. T., L. X., Z. L. and S. L. designed the experiment and wrote the manuscript. All authors reviewed the manuscript.

Supplementary Material

Supplementary figures and tables.

<http://www.thno.org/v07p3168s1.pdf>

Competing Interests

The authors have declared that no competing interest exists.

References

1. Reissmann, Siegmund. Cell penetration: scope and limitations by the application of cell-penetrating peptides. *J Pept Sci.* 2014; 20: 760-784.
2. Jones SW, Christison R, Bundell K, Voyce CJ, Brockbank SMV, Newham P, et al. Characterisation of cell-penetrating peptide-mediated peptide delivery. *Br J Pharmacol.* 2005; 145: 1093-1102.
3. Falanga A, Galdiero M, Galdiero S. Membranotropic Cell Penetrating Peptides: The Outstanding Journey. *Int J Mol Sci.* 2015; 16: 25323-25337.
4. Sayeh NA. Synthesis and evaluation of amphiphilic peptides as nanostructures and drug delivery tools. *Dissertations & Theses - Gradworks.* 2014; 21: 1680-1689.
5. Zhang D, Wang J, Xu D. Cell-penetrating peptides as noninvasive transmembrane vectors for the development of novel multifunctional drug-delivery systems. *J Control Release.* 2016; 229: 130-139.
6. Gilman NV. Analysis for Science Librarians of the 2015 Nobel Prize in Physiology or Medicine: The Life and Work of William C. Campbell, Satoshi Omura, and Youyou Tu. *Science & Technology Libraries.* 2016; 35: 35-58.
7. Liu Z, Deng M, Xiang J, Ma H, Hu W, Zhao Y, et al. A novel spider peptide toxin suppresses tumor growth through dual signaling pathways. *Curr Mol Med.* 2012; 12: 1350-1360.
8. Tan H, Ding X, Meng S, Liu C, Wang H, Xia L, et al. Antimicrobial potential of lycosin-I, a cationic and amphiphilic peptide from the venom of the spider *Lycosa singorensis*. *Curr Mol Med.* 2013; 13: 900-910.
9. Tan H, Luo W, Wei L, Chen B, Li W, Xiao L, et al. Quantifying the Distribution of the Stoichiometric Composition of Anticancer Peptide Lycosin-I on the Lipid Membrane with Single Molecule Spectroscopy. *J Phys Chem B.* 2016; 120: 3081-3088.

10. Her S, Jaffray DA, Allen C. Gold nanoparticles for applications in cancer radiotherapy: Mechanisms and recent advancements. *Adv Drug Deliv Rev.* 2015; 109: 84-101.
11. Vlieghe P, Lisowski V, Martinez J, Khrestchatsky M. Synthetic therapeutic peptides: science and market. *Drug Discov Today.* 2010; 15: 40-56.
12. Wei L, Yang Q, Xiao L. Tempo-spatially resolved cellular dynamics of human immunodeficiency virus transacting activator of transcription (Tat) peptide-modified nanocargos in living cells. *Nanoscale.* 2014; 6: 10207-10215.
13. Ye X, Zheng C, Chen J, Gao Y, Murray CB. Using binary surfactant mixtures to simultaneously improve the dimensional tunability and monodispersity in the seeded growth of gold nanorods. *Nano Lett.* 2013; 13: 765-771.
14. Wang X, Wang H, Wang Y, Yu X, Zhang S, Zhang Q, et al. A Facile Strategy to Prepare Dendrimer-stabilized Gold Nanorods with Sub-10-nm Size for Efficient Photothermal Cancer Therapy. *Sci Rep.* 2016; 6: 22764.
15. Yuan H, Fales AM, Vo-Dinh T. TAT peptide-functionalized gold nanostars: enhanced intracellular delivery and efficient NIR photothermal therapy using ultralow irradiance. *J Am Chem Soc.* 2012; 134: 11358-11361.
16. de la Fuente JM, Berry CC. Tat peptide as an efficient molecule to translocate gold nanoparticles into the cell nucleus. *Bioconj Chem.* 2005; 16: 1176-1180.
17. Nicol JR, Dixon D, Coulter JA. Gold nanoparticle surface functionalization: a necessary requirement in the development of novel nanotherapeutics. *Nanomedicine.* 2015; 10: 1315-1326.
18. Jain S, Hirst D, O'sullivan J. Gold nanoparticles as novel agents for cancer therapy. *Br J Radiol.* 2012; 85(1010): 101-113.
19. Eghtedari M, Liopo AV, Copland JA, Oraevsky AA, Motamedi M. Engineering of hetero-functional gold nanorods for the in vivo molecular targeting of breast cancer cells. *Nano Lett.* 2008; 9: 287-291.
20. Liu C-J, Wang C-H, Chien C-C, Yang T-Y, Chen S-T, Leng W-H, et al. Enhanced x-ray irradiation-induced cancer cell damage by gold nanoparticles treated by a new synthesis method of polyethylene glycol modification. *Nanotechnology.* 2008; 19: 295104.
21. Nativo P, Prior IA, Brust M. Uptake and intracellular fate of surface-modified gold nanoparticles. *ACS Nano.* 2008; 2: 1639-1644.
22. Park H, Tsutsumi H, Mihara H. Cell-selective intracellular drug delivery using doxorubicin and α -helical peptides conjugated to gold nanoparticles. *Biomaterials.* 2014; 35: 3480-3487.
23. Alkilany AM, Murphy CJ. Toxicity and cellular uptake of gold nanoparticles: what we have learned so far? *J Nanopart Res.* 2010; 12: 2313-2333.
24. Macia E, Ehrlich M, Massol R, Boucrot E, Brunner C, Kirchhausen T. Dynasore, a cell-permeable inhibitor of dynamin. *Dev Cell.* 2006; 10: 839-850.
25. Gratton SE, Ropp PA, Pohlhaus PD, Luft JC, Madden VJ, Napier ME, et al. The effect of particle design on cellular internalization pathways. *Proc Natl Acad Sci USA.* 2008; 105: 11613-11618.
26. Arvizo RR, Miranda OR, Moyano DF, Walden CA, Giri K, Bhattacharya R, et al. Modulating pharmacokinetics, tumor uptake and biodistribution by engineered nanoparticles. *PLoS One.* 2011; 6(9): e24374.
27. Chanda N, Kattumuri V, Shukla R, Zambre A, Katti K, Upendran A, et al. Bombesin functionalized gold nanoparticles show in vitro and in vivo cancer receptor specificity. *Proc Natl Acad Sci USA.* 2010; 107: 8760-8765.
28. Villanueva A, Canete M, Roca AG, Calero M, Veintemillas-Verdaguer S, Serna CJ, et al. The influence of surface functionalization on the enhanced internalization of magnetic nanoparticles in cancer cells. *Nanotechnology.* 2009; 20: 115103.
29. Ojea-Jimeñez I, García-Fernández L, Lorenzo J, Puentes VF. Facile preparation of cationic gold nanoparticle-bioconjugates for cell penetration and nuclear targeting. *ACS Nano.* 2012; 6: 7692-7702.
30. Olson ES, Jiang T, Aguilera TA, Nguyen QT, Ellies LG, Scadeng M, et al. Activatable cell penetrating peptides linked to nanoparticles as dual probes for in vivo fluorescence and MR imaging of proteases. *Proc Natl Acad Sci USA.* 2010; 107: 4311-4316.
31. Jiang T, Zhang Z, Zhang Y, Lv H, Zhou J, Li C, et al. Dual-functional liposomes based on pH-responsive cell-penetrating peptide and hyaluronic acid for tumor-targeted anticancer drug delivery. *Biomaterials.* 2012; 33: 9246-9258.
32. Park H, Tsutsumi H, Mihara H. Cell penetration and cell-selective drug delivery using α -helix peptides conjugated with gold nanoparticles. *Biomaterials.* 2013; 34: 4872-4879.
33. Troeira HS, Huang YH, Chaousis S, Wang CK, Craik DJ. Anticancer and toxic properties of cyclotides are dependent on phosphatidylethanolamine phospholipid targeting. *Chembiochem.* 2014; 15: 1956.
34. Riedl S, Zweytick D, Lohner K. Riedl S, Zweytick D, Lohner K. Membrane-active host defense peptides - Challenges and perspectives for the development of novel anticancer drugs. *Chem Phys Lipids.* 2011; 164: 766-781.
35. Diana G, Salomé VA, Castanho MARB. From antimicrobial to anticancer peptides. A review. *Front Microbiol.* 2013; 4: 294.
36. Wang C, Sun A, Qiao Y, Zhang P, Ma L, Su M. Cationic surface modification of gold nanoparticles for enhanced cellular uptake and X-ray radiation therapy. *J Mater Chem B Mater Biol Med.* 2015; 3: 7372-7376.
37. Chien CC, Chen HH, Lai SF, Hwu Y, Petibois C, Yang CS, et al. X-ray imaging of tumor growth in live mice by detecting gold-nanoparticle-loaded cells. *Sci Rep.* 2012; 2(8): 610.
38. Huang X, El-Sayed IH, Qian W, El-Sayed MA. Cancer cell imaging and photothermal therapy in the near-infrared region by using gold nanorods. *J Am Chem Soc.* 2006; 128: 2115-2120.
39. Huang X, El-Sayed MA. Gold nanoparticles: optical properties and implementations in cancer diagnosis and photothermal therapy. *J Adv Res.* 2010; 1: 13-28.
40. Choi WI, Kim J-Y, Kang C, Byeon CC, Kim YH, Tae G. Tumor regression in vivo by photothermal therapy based on gold-nanorod-loaded, functional nanocarriers. *ACS Nano.* 2011; 5: 1995-2003.
41. Helmchen F, Denk W. Deep tissue two-photon microscopy. *Nat Methods.* 2005; 2: 932-940.